Acta Crystallographica Section D
Biological Crystallography
ISSN 0907-4449

Atomic resolution studies of haloalkane dehalogenases DhaA04, DhaA14 and DhaA15 with engineered access tunnels

A. Stsiapanava,[a] J. Dohnalek,[b] J. A. Gavira,[c] M. Kuty,[a,d] T. Koudelakova,[e] J. Damborsky[e] and I. Kuta Smatanova[a,d]*

[a]Institute of Physical Biology, University of South Bohemia, Ceske Budejovice, Zamek 136, 373 33 Nove Hrady, Czech Republic, [b]Institute of Macromolecular Chemistry, Academy of Science of the Czech Republic, Heyrovskeho nam. 2, 162 00 Prague 6, Czech Republic, [c]Laboratorio de Estudios Cristalográficos, IACT (CSIC–Universidad de Granada), P. T. Ciencias de la Salud, Granada 18100, Spain, [d]Institute of Systems Biology and Ecology Academy of Science of the Czech Republic, Zamek 136, 373 33 Nove Hrady, Czech Republic, and [e]Loschmidt Laboratories, Institute of Experimental Biology and Research Centre for Toxic Compounds in the Environment, Faculty of Science, Masaryk University, Kamenice 5/A4, 62500 Brno, Czech Republic

Correspondence e-mail: ivanaks@seznam.cz

Received 9 June 2010
Accepted 8 July 2010

PDB References: DhaA04 (C176Y), 3fbw; DhaA14 (I135F), 3g9x; DhaA15 (C176Y + I135F), 3fwh.

The haloalkane dehalogenase DhaA from *Rhodococcus rhodochrous* NCIMB 13064 is a bacterial enzyme that shows catalytic activity for the hydrolytic degradation of the highly toxic industrial pollutant 1,2,3-trichloropropane (TCP). Mutagenesis focused on the access tunnels of DhaA produced protein variants with significantly improved activity towards TCP. Three mutants of DhaA named DhaA04 (C176Y), DhaA14 (I135F) and DhaA15 (C176Y + I135F) were constructed in order to study the functional relevance of the tunnels connecting the buried active site of the protein with the surrounding solvent. All three protein variants were crystallized using the sitting-drop vapour-diffusion technique. The crystals of DhaA04 belonged to the orthorhombic space group $P2_12_12_1$, while the crystals of DhaA14 and DhaA15 had triclinic symmetry in space group $P1$. The crystal structures of DhaA04, DhaA14 and DhaA15 with ligands present in the active site were solved and refined using diffraction data to 1.23, 0.95 and 1.22 Å, resolution, respectively. Structural comparisons of the wild type and the three mutants suggest that the tunnels play a key role in the processes of ligand exchange between the buried active site and the surrounding solvent.

1. Introduction

Haloalkane dehalogenases (EC 3.8.1.5), which belong to the α/β-hydrolase fold family (Ollis *et al.*, 1992; Nardini & Dijsktra, 1999), catalyze the hydrolytic conversion of a broad spectrum of haloalkanes to the corresponding alcohols (Janssen, 2004). There is no experimental evidence suggesting the involvement of cofactors or metal ions in the catalytic activity of these enzymes (Janssen *et al.*, 1994). The cleavage of the carbon–halogen bonds in halogenated compounds, which can be environmental pollutants, is a key step in their decontamination (Janssen *et al.*, 2005). Therefore, these enzymes can be used as biocatalysts in environmental biotechnology (Stucki & Thuer, 1995; Swanson, 1999; Janssen & Schanstra, 1994). Moreover, haloalkane dehalogenases have been applied in industrial biocatalysis (Prokop *et al.*, 2004), as active components of biosensors (Campbell *et al.*, 2006; Bidmanova *et al.*, submitted) and in decontamination mixtures for warfare agents (Prokop *et al.*, 2005, 2006). An attractive application of haloalkane dehalogenases is in the degradation of 1,2,3-trichloropropane (TCP). TCP is a toxic industrial pollutant that is resistant to biological degradation (Bosma *et al.*, 1999). The haloalkane dehalogenase DhaA from the Gram-positive bacterium *Rhodococcus rhodochrous* NCIMB 13064 (Kulakova *et al.*, 1997) can slowly degrade TCP (Schindler *et al.*,

1999; Bosma *et al.*, 1999), although the catalytic efficiency of the native enzyme is too low for the use of DhaA in biotechnological processes. Protein engineering has been used for the construction and evolution of modified DhaA with improved catalytic properties towards TCP (Gray *et al.*, 2001; Bosma *et al.*, 2002; Pavlova *et al.*, 2009).

Structurally, DhaA consists of two domains: an α/β-hydrolase domain and a helical cap domain. The active-site cavity is buried in the protein core between the domains (Newman *et al.*, 1999) and is connected to the surrounding solvent by the main tunnel and the side (slot) tunnel (Otyepka & Damborsky, 2002). The side tunnel may present a secondary path for substrates, products and water molecules (Oakley *et al.*, 2003). Bosma *et al.* (2002) reported a mutant carrying the substitution C176Y, named M1 by Bosma and coworkers and DhaA04 in this work, which shows threefold improved catalytic efficiency towards TCP compared with the wild-type enzyme. Banas *et al.* (2006) used molecular simulation to study the mechanism of the improved catalysis by this mutant and proposed that the side chain of residue 176 narrows the main tunnel, possibly making the side tunnel a preferred route in DhaA04. The mutant enzyme DhaA14, which carries an I135F mutation in the side tunnel, was constructed by site-directed mutagenesis in order to reveal the importance of the side tunnel in catalysis. DhaA15 carries both of these mutations (C176Y + I135F) in the main tunnel and the side tunnel.

In this work, we report and compare the structures of three DhaA mutants at atomic resolution in order to explore the effect of mutations on the enzymatic activity of modified proteins from a structural perspective.

Table 1
Data-collection and refinement statistics.

Values in parentheses are for the highest resolution shell.

	DhaA04	DhaA14	DhaA15
Data collection			
Resolution range (Å)	100–1.23 (1.25–1.23)	19.86–0.95	20–1.22
Unit-cell parameters (Å, °)	a = 42.68, b = 76.30, c = 93.10, $\alpha = \beta = \gamma$ = 90	a = 42.74, b = 44.40, c = 46.62, α = 115.5, β = 97.9, γ = 109.5	a = 42.52, b = 44.37, c = 46.54, α = 115.5, β = 98.4, γ = 109.6
Space group	$P2_12_12_1$	$P1$	$P1$
Redundancy	7.4 (5.7)	5.8 (4.0)	3.4 (2.1)
Measured reflections	652804	948271	261056
Unique reflections	88814	162574	77114
Completeness (%)	100 (99.9)	94.2 (90.6)	90.7 (75.6)
$R_{\rm merge}$† (%)	5.6 (58.1)	5.9 (41.8)	5.0 (17.9)
$I/\sigma(I)$	25.6 (4.2)	26.4 (4.4)	29.6 (6.8)
Refinement			
No. of reflections used for refinement	88731	163371	77113
Maximum resolution (Å)	1.23	0.95	1.22
$R_{\rm work}$‡/$R_{\rm free}$§ (%)	13.7/16.7	11.5/13.7	13.2/16.2
No. of non-H atoms	3163	2901	3367
No. of protein atoms	2692	2372	2725
No. of ligand atoms	9	4	4
No. of acetate ions	0	1	1
No. of magnesium ions	2	0	0
No. of chloride ions	6	1	2
No. of water molecules	454	520	632
No. of restraints	37060	32628	13225
Average B factor (Å^2)	13.4	13.2	13.1
R.m.s. deviations			
Bond lengths (Å)	0.011	0.015	0.014
Bond angles	0.028 Å	0.031 Å	1.605°
PDB code	3fbw	3g9x	3fwh

† $R_{\rm merge} = \sum_{hkl}\sum_i |I_i(hkl) - \langle I(hkl)\rangle| / \sum_{hkl}\sum_i I_i(hkl)$, where $I_i(hkl)$ is the intensity of the ith measurement of reflection hkl and $\langle I(hkl)\rangle$ is the average intensity of this reflection. ‡ $R = \sum_{hkl} ||F_{\rm obs}| - |F_{\rm calc}|| / \sum_{hkl} |F_{\rm obs}|$. § $R_{\rm free}$ was monitored using 5% of the reflection data that were excluded from refinement.

2. Materials and methods

2.1. Protein crystallization

The DhaA mutants were expressed, purified and crystallized as described previously (Stsiapanava *et al.*, 2008). The sitting-drop vapour-diffusion technique (Ducruix & Giegé, 1999) was used to screen and optimize crystallization conditions for all three proteins. 1 µl DhaA04 mutant protein at a concentration of 15–18 mg ml^{-1} in 50 m*M* Tris–HCl buffer pH 7.5 was mixed with an equal volume of reservoir solution consisting of 80 m*M* Bicine pH 9.0, 8%(*w*/*v*) PEG 8000 and 80 m*M* $MgCl_2$. Crystals appeared at room temperature and grew to dimensions of about 0.20 × 0.15 × 0.06 mm within 7 d. Plate-shaped crystals with dimensions of 0.16 × 0.06 × 0.02 mm for DhaA14 and 0.17 × 0.07 × 0.02 mm for DhaA15 grew within 5 d at a temperature of 277 K in drops containing 1 µl protein solution and 1 µl reservoir solution composed of 25%(*w*/*v*) PEG 4000, 8% 2-propanol and 100 m*M* sodium acetate. DhaA14 and DhaA15 were crystallized using protein at a concentration of 7–10 mg ml^{-1} in 50 m*M* Tris–HCl buffer pH 7.5. The drops were equilibrated against 700 µl reservoir solution for DhaA04 and 600 µl reservoir solution for DhaA14 and DhaA15.

2.2. Data collection and structure solution

All data sets were collected on beamline X11 at EMBL/DESY, Hamburg with a monochromatic fixed wavelength of 0.81 Å using a MAR CCD 165 mm detector for the DhaA04 and DhaA14 crystals and a MAR 555 flat-panel detector for the DhaA15 crystals. All crystals were mounted in a nylon loop (Teng, 1990) and flash-frozen in a nitrogen stream at 100 K without additional cryoprotection. The diffraction data for DhaA04 were collected in two steps. 159 low-resolution images (30–2.3 Å) were recorded with an oscillation angle of 1° and a crystal-to-detector distance of 200 mm. A high-

resolution set of 318 images (30–1.2 Å) was collected with an oscillation angle of 0.5° and a crystal-to-detector distance of 85 mm. The DhaA14 data were collected in three steps. 360 low-resolution images (30–2.2 Å) were recorded using an oscillation angle of 1° and a crystal-to-detector distance of 210 mm. A 1° oscillation angle and a crystal-to-detector distance of 100 mm were used to collect 720 medium-resolution images (30–1.25 Å). Using a 0.5° oscillation angle, 720 frames were collected for the high-resolution set (30–0.95 Å) with the crystal-to-detector distance set to 50 mm. A single data set was collected for DhaA15 with a 0.5° oscillation angle and a crystal-to-detector distance of 171 mm. All data sets were indexed, integrated and scaled using the *HKL*-2000 program package (Otwinowski & Minor, 1997). The data-collection statistics are summarized in Table 1.

2.3. Structure refinement

The structures of DhaA04, DhaA14 and DhaA15 were solved by the molecular-replacement method using the coordinates of haloalkane dehalogenase from *R. rhodochrous* (PDB code 1bn6; Newman *et al.*, 1999), excluding waters, as a search model. The molecular replacement solution was found using *MOLREP* (Vagin & Teplyakov, 1997).

The structure of DhaA04 was refined with the use of *SHELXL* (Sheldrick, 2008) and manual building steps were performed in *Coot* (Emsley *et al.*, 2010); other data and coordinate manipulations were performed in the *CCP*4 program package (Collaborative Computational Project, Number 4, 1994). After the protein and partial solvent structure had been refined, the difference Fourier of the active site was interpreted. An analysis of the distances of the peaks within the cavity was used in searches for small molecules in the CSD database (Allen, 2002) and, in parallel, ligands available from the PDB were included in the survey. Benzoic acid was evaluated as being the most likely candidate and was refined with a geometric library based on small-molecule crystallographic data. The presence of anomalous difference maxima and the typical distances of Cl^-—HN contacts were used to assess the nature of the chloride ions in the structure. The presence of the ion as part of the small ligand within the active site was excluded by the close proximity of the corresponding electron-density maxima, the distance between which was too short for the common bond length of a non-H covalent bond. The joint occupancy refinement implemented in *SHELXL* was applied for the alternative conformations surrounding the active site and the corresponding ligands, resulting in an occupancy ratio of 0.45:0.55. DELU and SIMU restraints were used as implemented in *SHELXL*; the ISOR restraint was applied to waters with isotropic ADPs greater than the average for the whole structure. Anisotropic atomic displacement parameters were refined for all protein and ligand atoms and ions and for water O atoms with refined isotropic ADPs below the average solvent value.

Subsequent refinement of DhaA14 was conducted using the *SHELXL* program and refinement of the DhaA15 structure was carried out using *REFMAC*5 from the *CCP*4 suite (Murshudov *et al.*, 1997). After rigid-body refinement and several cycles of restrained isotropic ADP refinement, manual building of the models against the electron-density maps was conducted with *Coot*. The difference in electron density in the active sites of both mutants was interpreted as a molecule of 2-propanol from the crystallization solution and a chloride ion. The ISOR restraint was applied to all waters and ligands of DhaA14. For water O atoms of DhaA15 the isotropic ADPs were kept if their values were higher than the average isotropic value for the whole structure. Anisotropic ADPs were refined for all protein atoms of DhaA14 and for all protein and ligand atoms of DhaA15.

The introduction of combined anisotropic/isotropic ADP refinement of DhaA04, DhaA14 and DhaA15 resulted in a lowering of the R and $R_{\rm free}$ statistics from $R = 0.164$ and $R_{\rm free} = 0.177$ to $R = 0.133$ and $R_{\rm free} = 0.157$ for DhaA04, from $R = 0.171$ and $R_{\rm free} = 0.186$ to $R = 0.14$ and $R_{\rm free} = 0.16$ for DhaA14 and from $R = 0.194$ and $R_{\rm free} = 0.213$ to $R = 0.18$ and $R_{\rm free} = 0.206$ for DhaA15 (Brünger, 1993). The structure-refinement statistics are compiled in Table 1.

2.4. Model validation and deposition

The quality of the structure models with respect to the experimental data was assessed using the program *SFCHECK* (Vaguine *et al.*, 1999). Geometric parameters were validated using the internal tools of *Coot* and the *MolProbity* service (Chen *et al.*, 2010). 97% of the residues in the structures of DhaA04, DhaA14 and DhaA15 lie in allowed regions of the Ramachandran plot, with one outlier in each mutant. The Ramachandran outlier is caused by strain exerted on the main chain of the protein in the region of Pro42. The structures and

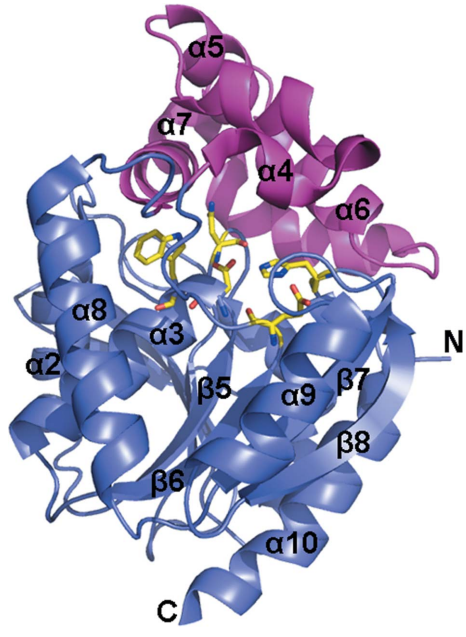

Figure 1
Cartoon representation of the DhaA structure. The α/β-hydrolase core domain is shown in blue and the helical cap domain is shown in magenta. Catalytic pentad residues are shown in yellow stick representation. This figure was prepared using *PyMOL* (DeLano, 2002).

original diffraction intensities were deposited in the Protein Data Bank under the following accession codes: DhaA04 (C176Y), 3fbw; DhaA14 (I135F), 3g9x; DhaA15 (C176Y, I135F), 3fwh.

2.5. Tunnel calculation and visualization

The pathways corresponding to the main and the side tunnels in wild-type DhaA (Newman *et al.*, 1999), DhaA04, DhaA14 and DhaA15 were calculated using the program *CAVER* (Petrek *et al.*, 2006) and visualized using the *PyMOL* plugin (DeLano, 2002). The (x, y, z) coordinates (−5.983, −0.144, 16.683) located in the active-site cavity were used as the starting point for calculation of pathways in the DhaA04 mutant and equivalent positions were used in the structures of other mutants. The structures were superimposed in *PyMOL* (DeLano, 2002) for these calculations.

3. Results and discussion

3.1. Overall structure of DhaA mutants

The crystal structures of DhaA04, DhaA14 and DhaA15 were determined. The structure of DhaA04 is most likely to correspond to a complex with benzoic acid, while those of DhaA14 and DhaA15 contained 2-propanol in their active sites. The DhaA04 data allowed the localization of residues 3–295, while for DhaA14 and DhaA15 electron density was clear for residues 4–297 and 2–297, respectively. The overall structure of the DhaA mutants is similar to that of haloalkane dehalogenase from *R. rhodochrous* as previously described by Newman *et al.* (1999). The DhaA protein is composed of an α/β-hydrolase core domain and a helical cap domain (Fig. 1). The core domain includes an eight-stranded β-sheet and six α-helices ($\beta1$–$\beta2$–$\beta3$–$\alpha1$–$\beta4$–$\alpha2$–$\beta5$–$\alpha3$–$\beta6$, $\alpha8$–$\beta7$–$\alpha9$–$\beta8$–$\alpha10$; Chovancova *et al.*, 2007). The β-sheet is mostly parallel, with a single antiparallel β-strand ($\beta2$). The α/β-hydrolase domain forms a hydrophobic core that contains catalytic residues typical of haloalkane dehalogenases. The active-site cavity is located between the core and cap domains. Asn41 is one of the pair of amino acids forming the halide binding site and is positioned in the loop joining β-strand $\beta3$ and α-helix $\alpha1$. The nucleophile Asp106 and the halide-stabilizing Trp107 are located in the loop following β-strand $\beta5$. The catalytic base His272 is located in the loop between β-strand $\beta8$ and the C-terminal α-helix $\alpha10$. The acidic residue Glu130 is located in the loop following β-strand $\beta6$. The cap domain comprises of five α-helices ($\alpha4$–$\alpha5'$–$\alpha5$–$\alpha6$–$\alpha7$) inserted between β-strand $\beta6$ and α-helix $\alpha8$ of the α/β-hydrolase fold (Chovancova *et al.*, 2007).

3.2. Structural comparison of DhaA mutants

The coordinate root-mean-square deviation (r.m.s.d.) of 291 aligned residues of the three mutants superimposed with *SSM* (Krissinel & Henrick, 2004) is 0.39 Å. While DhaA14 and DhaA15 superimpose very well, with an r.m.s.d. of 0.1 Å, superposition of DhaA14 on DhaA04 and of DhaA15 on DhaA04 reveals deviations of 0.46 and 0.49 Å, respectively. The most significant deviations in the DhaA04 structure compared with the structures of DhaA14 and DhaA15 are observed in the flexible parts of the protein. In DhaA04, residues 153–156, which form a loop between the $\alpha4$ and $\alpha5'$ helices of the cap domain, have two alternative conformations. Another flexible loop in the DhaA proteins connects the $\beta2$ and $\beta3$ strands of the core domain and has an r.m.s.d. of more than 2 Å for the 30 and 31 C^{α} alternative positions in DhaA04. Differences in the position of the C^{α} atom of Asp106 are comparable when DhaA04 is compared with DhaA14 and with DhaA15, while the position of the C^{α} atom of Trp107 differs by less than 0.1 Å in all possible superpositions of the mutants.

Two magnesium cations and six chloride anions from the crystallization solution are present in the structure of DhaA04. The magnesium ions and five chloride anions are bound on the protein surface and one chloride ion is located in the active site. Difference electron density in the active site indicated the presence of a small ligand with a partial occupancy alternating with the presence of the chloride ion. After thorough analysis of the electron-density peaks and a search for a corresponding molecule, a molecule of benzoic acid was modelled in this region. The origin of the benzoic acid or a stereochemically identical molecule in the structure of DhaA04 is unclear. Since benzoate-like compounds were not used during crystallization, we suppose that the ligand bound to the structure of DhaA is a metabolite from cultivation of the cells or an impurity from the chemicals in the cultivation medium. The mutation of the cysteine in position 176 to the bulky tyrosine blocks the main tunnel and contributes to the stabilization of the ligand inside the active-site cavity.

The structures of both DhaA14 and DhaA15 contain one chloride ion and one 2-propanol molecule in the active-site cavity. The 2-propanol and the chloride anions most probably bind to the protein from the crystallization medium (see §2). In the structures of DhaA14 and DhaA15 an acetate ion was found close to the C-terminus. The acetate ion is hydrogen bonded to the imidazole N atoms of His59 and His294 to stabilize the flexible His tag and the loop between strand $\beta4$ and helix $\alpha5$ of these two mutants. One O atom of the acetate ion also binds to the side-chain amino group of Lys124 in the loop between helix $\alpha8$ and strand $\beta7$ and to the hydroxyl group of Thr33 in the loop between the $\beta2$ and $\beta3$ strands and coordinates these two loops. In the case of DhaA14 an acetate ion with half occupancy alternates with two water molecules that also have 0.5 occupancies.

3.3. Analysis of active sites

All three structures have electron-density peaks present in the active site that can be relatively well interpreted as ligands, water molecules and ions. A chloride ion was identified in the active site of all of the mutants. Its location and links to the halide-binding amino acids are almost identical in all three cases. The average distances between the chloride ion in the active site and the N atoms Asn41 $N^{\delta2}$ and Trp107 $N^{\varepsilon1}$ are 3.38 and 3.21 Å, respectively.

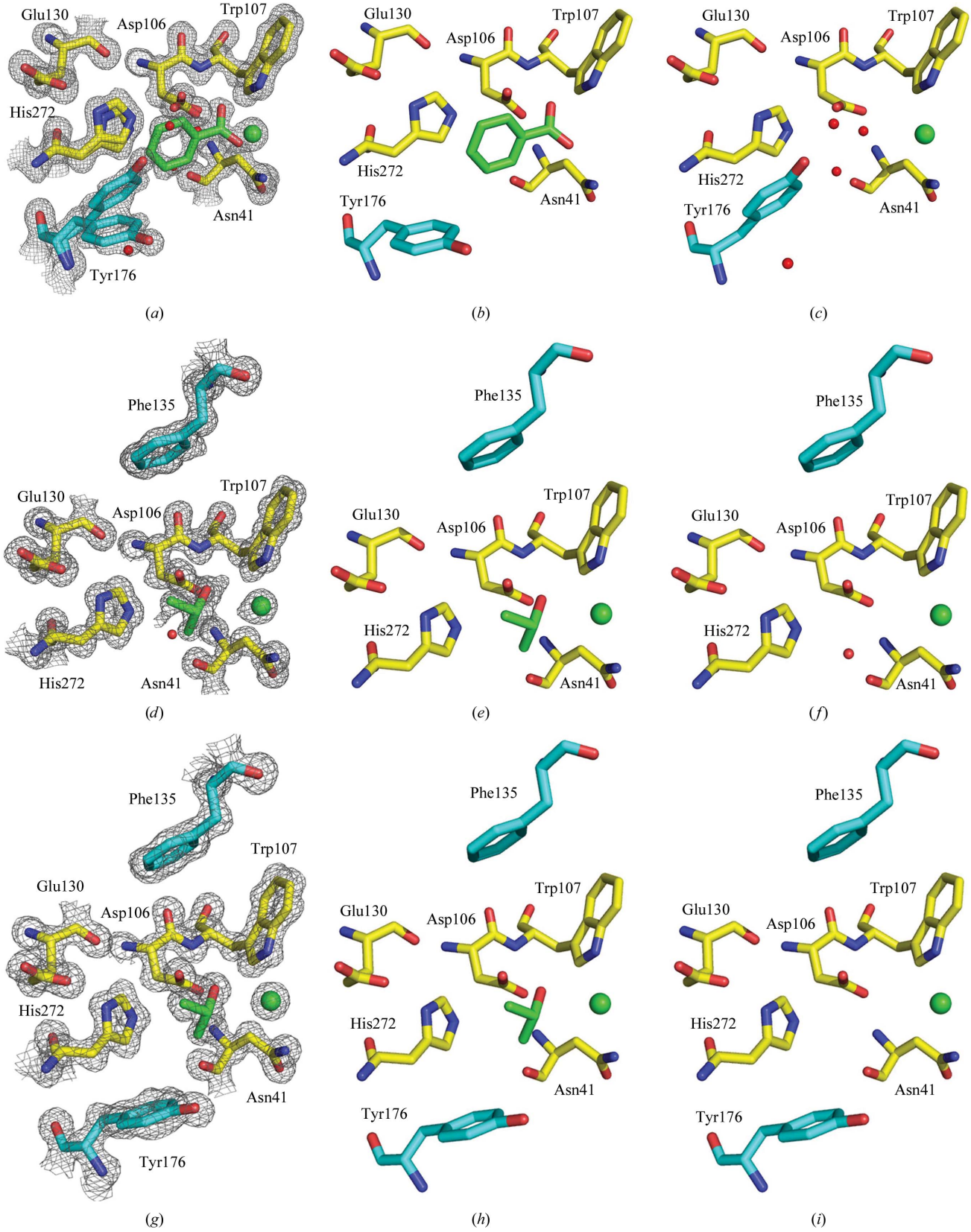

Figure 2
The active site of mutants with ligands. ($2F_o - F_c$) electron density (contoured at 1σ) around the active site of DhaA04 (*a*), DhaA14 (*d*) and DhaA15 (*g*) is shown as a grey mesh. Stick representations of the DhaA04 active site are shown with (*b*) and without (*c*) benzoic acid. Stick representations of the DhaA14 active site are shown with (*e*) and without (*f*) 2-propanol. Stick representations of the DhaA15 active site are shown with (*h*) and without (*i*) 2-propanol. The catalytic pentad is coloured yellow, the ligands are in green, the mutated residues are shown in cyan and the green sphere represents chloride anions; red spheres represent the O atoms of water molecules. This figure was prepared using *PyMOL* (DeLano, 2002).

The ligand in the active site of DhaA04 was interpreted as benzoic acid (or a similar compound with identical stereochemistry) with an occupancy of 0.45 alternating with a chloride ion and three water molecules with an occupancy of 0.55 (Fig. 2*a*). The catalytic site residues Asp106, His272 and the mutated Tyr176 are modelled in two possible conformations depending on the molecules that occupy the active site. The benzoic acid or chloride-ion positions in the active site are stabilized by interactions with Asn41 $N^{\delta2}$ and Trp107 $N^{\varepsilon1}$ of the halide-binding site. At the same time, the O^{2} atom of benzoic acid is very likely to form hydrogen bonds to the $O^{\delta1}$ and $O^{\delta2}$ atoms of the conserved Asp106 (alternative *A*; Fig. 2*b*). Asp106*A* $O^{\delta1}$ determines the position of His272 (alternative *B*) by association of the acidic oxygen $O^{\delta1}$ with $N^{\varepsilon1}$ of the imidazole ring. The third member of the catalytic triad, Glu130, stabilizes His272 through the connection of the acidic oxygen $O^{\varepsilon1}$ to the second N atom of the imidazole ring. In the absence of benzoic acid, Asp106 (alternative *B*) and His272 (alternative *A*) change conformations and the empty active-site cavity is occupied by water molecules and the chloride ion (Fig. 2*c*). The water molecules interact with Asp106 $O^{\delta1}$ (alternative *B*) and the hydroxyl groups of Tyr176 and Tyr273. The mutated residue Tyr176 is located at the mouth of the main tunnel and has two alternative conformations. The presence of the ligand in the active site causes the residue to reorient and bend its side chain towards the main tunnel and protein surface (Fig. 2*b*). The second conformation places the Tyr176 side chain into the cavity but still allows the chloride ion and water molecules to be bound in the active site (Fig. 2*c*).

There is an ambiguity in the interpretation of the electron density in the active site of DhaA14. A careful analysis reveals that the modelled 2-propanol and water molecule placed into the active-site cavity could be replaced by a larger ligand of unknown identity (Fig. 2*d*).

In the case of DhaA15, 2-propanol and a chloride ion were found in the active-site cavity but no water molecules were found (Fig. 2*g*). A hydroxyl group of 2-propanol in DhaA15 makes a hydrogen bond to Asp106 $O^{\delta1}$ as in DhaA14. The distance between the O atom of the hydroxyl group of 2-propanol and the chloride ion is 3.0 Å, with occupancies of 0.7 and 0.9 in the structures of DhaA14 and DhaA15, respectively. Hence, it is hard to distinguish whether 2-propanol and the chloride ion are present in the active site simultaneously (Figs. 2*e* and 2*h*) or not (Figs. 2*f* and 2*i*). In general, the presence or absence of 2-propanol in the active site does not influence the geometry of the catalytic residues and the mutated Phe135 of the side tunnel.

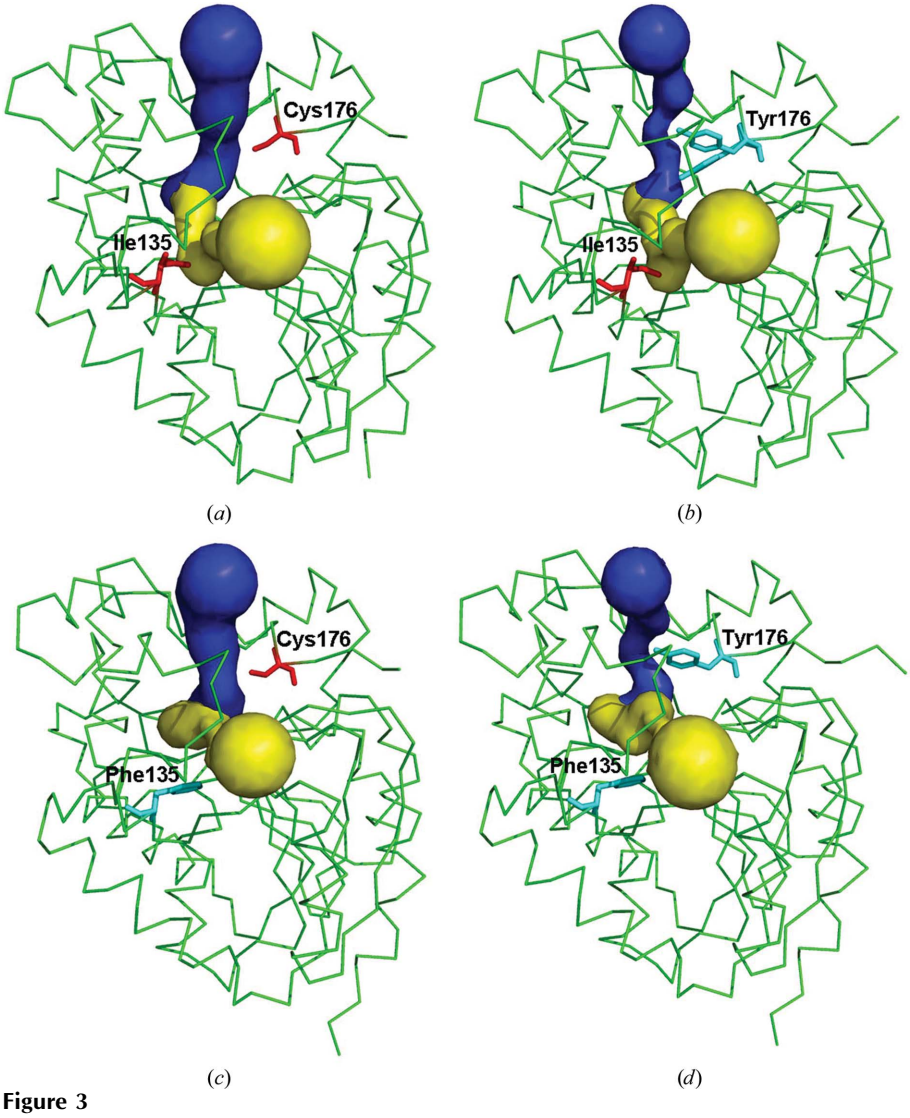

Figure 3
Ribbon representations of the structures of wild-type DhaA (*a*), DhaA04 (*b*), DhaA14 (*c*) and DhaA15 (*d*) with the main tunnel shown in blue and the side tunnel in yellow. The residues selected for mutagenesis are shown as red sticks; the mutated residues are represented by cyan sticks. The tunnels were calculated using *CAVER* (Petrek *et al.*, 2006) and visualized in *PyMOL* (DeLano, 2002).

3.4. Analysis of access tunnels

DhaA proteins have several tunnels that connect the active-site cavity with bulk solvent and that take part in the exchange of ligands and solvent (Klvana *et al.*, 2009). The substitutions introduced into the DhaA mutants modify the mouths of two access tunnels: the main tunnel and the side tunnel. It has been shown experimentally that modification of the size of the access tunnels changes the kinetics of the overall biochemical reaction as well as of individual reaction steps (Pavlova *et al.*, 2009). The narrowing of the access tunnels in DhaA enhanced the activity towards TCP by decreasing the acces-

sibility of the active site to water molecules, thereby promoting the formation of the activated complex. For larger substrates, the narrowing of the access tunnel can have the opposite effect and results in a reduction in activity owing to the slower release of products. It can be envisaged that larger ligands will be stabilized in the active site owing to mutations blocking the access tunnels.

The main tunnel is located between the α4 and α5 helices of the cap domain and is formed by nonpolar residues such as Ala145, Phe144, Phe149, Phe168, Ala172 and Cys176, and polar residues such as Thr148 and Lys175 (Petrek *et al.*, 2006). The most mobile part of the structures described here occurs in a loop joining the helices to the main tunnel residues. It is possible that the motion of this region and of the Lys175 side chain allows the access of substrates with different dimensions into the active-site cavity through the main tunnel. The flexible side chain of Lys175 in the main tunnel adopts two conformations in the case of DhaA04. In DhaA04 and DhaA15 the longer polar Tyr side chain is substituted for the nonpolar Cys176. In the DhaA04 structure the side chain of Tyr176 is flexible and the $C^{\alpha}-C^{\beta}-C^{\gamma}$ bond angle changes from 114.2° (alternative *A*) to 130.4° (alternative *B*) (Figs. 2*a* and 3*b*). The occupancies of the *A* and *B* alternatives of DhaA04 Tyr176 are 0.45 and 0.55, respectively. Tyr176 of DhaA15 has only one conformation, with a $C^{\alpha}-C^{\beta}-C^{\gamma}$ bond angle of 111.7° (Figs. 2*g* and Fig. 3*d*). In the presence of benzoic acid in the active site of DhaA04 and 2-propanol in the active site of DhaA15, the side chain of Tyr176 turns towards the entrance of the main tunnel, resulting in partial closure of this tunnel (Figs. 2*b*, 2*h*, 3*b* and 3*d*). With the chloride ion and three water molecules present in the active site of DhaA04, the side chain of Tyr176 is placed closer to the cavity, which opens the main tunnel for ligand entry (Figs. 2*c* and Fig. 3*b*). One further water molecule is located in the open tunnel.

The smaller side tunnel can be found between the α4 helix of the cap domain and the loops connecting helix α4 to strand β3 of the core domain and strand β3 to helix α8. The side tunnel is surrounded by the nonpolar amino acids Ile132, Ile135, Trp141, Pro142, Leu246 and Val245, and the polar residues Arg133 and Glu140 (Petrek *et al.*, 2006). The most flexible residues of this tunnel are Glu140, which is found in two conformations in the structures of DhaA04, DhaA14 and DhaA15, and Arg133, which has one conformer in DhaA04 and two and three conformers in DhaA14 and DhaA15, respectively. The mobility of these residues, as reflected by their different conformations, is needed for the exchange of ligands through the side tunnel. In DhaA14 and DhaA15 Ile135 was mutated to Phe with an almost identical position in both mutants (Figs. 2*d*, 2*g*, 3*c* and 3*d*). When DhaA15 is superimposed on DhaA14 the position of Phe135 C^{α} is shifted by 0.09 Å and the r.m.s.d. for the superimposed side-chain atoms is 0.1 Å. The presence of 2-propanol, or alternatively a water molecule, in the active site does not influence the conformation of Phe135 in the structure of DhaA14 (Figs. 2*e*, 2*f* and 3*c*). The bulky nonpolar side chain of Phe135 adopts a strained conformation in the small space among the surrounding amino acids. The $C^{\alpha}-C^{\beta}-C^{\gamma}$ bond angle in this conformation is 112.4°. The ring of the Phe135 side chain blocks the small side tunnel in DhaA14 and DhaA15 (Figs. 3*c* and 3*d*). The constriction of the access tunnels arising from the mutations is not sufficient to prevent access of water molecules to the active site, but exchange of the solvent between the protein core and the surface will be significantly affected.

4. Conclusions

The crystal structures of the three haloalkane dehalogenase mutants DhaA04 (C176Y), DhaA14 (I135F) and DhaA15 (C176Y + I135F) were solved by the molecular-replacement method at resolutions of 1.23, 0.95 and 1.22 Å, respectively.

The crystals of DhaA04 were grown in the presence of magnesium chloride and Mg^{2+} ions were identified in the structure in positions close to the protein surface. Acetate ions included in the precipitating agents used for DhaA14 and DhaA15 are bound to their flexible C-termini. The active site of DhaA04 contains a molecule of a ligand best represented by benzoic acid and of unknown origin. The 2-propanol molecule detected in the structures of DhaA14 and DhaA15 entered the active site of these mutants from the crystallization solution. 2-Propanol structurally and chemically resembles the alcohol product of the hydrolytic dehalogenation. Therefore, the positions of 2-propanol and the chloride ion from the protein buffer in the active sites of DhaA14 and DhaA15 allow the modelling of dehalogenation products in the active site before their release from the cavity. No water molecules are observed in the presence of benzoic acid or 2-propanol. In the absence of these ligands, three and one water molecule(s) fill the empty space in the active sites of DhaA04 and DhaA14, respectively. In the case of the active site of DhaA15 no electron density for water molecules was observed. The position of the chloride ion in the active site is approximately the same in all three described structures. The structure of two halide-stabilizing and three catalytic residues of the three proteins is highly conserved, showing the minimal effect of the introduced mutations on the architecture of the active site.

Apparent differences among three mutants are noted in the most flexible parts of the structures, such as the loop connecting strands β2 and β3 of the core domain and the loop between helices α4 and α5′ of the cap domain. The latter loop joins the helices to the main tunnel residues. Some residues surrounding the main tunnel and the side tunnel in the DhaA structures can change conformation, which may influence the process of substrate entry and product egress. The point mutations in DhaA04, DhaA14 and DhaA15 lead to changes in the anatomy of the main tunnel, side tunnel and both the main tunnel and the side tunnel, respectively. The substitution of Cys176 by Tyr in DhaA04 and DhaA15 partially blocks the main tunnel when the active site is occupied by benzoic acid or 2-propanol. At the same time, the side chain of Tyr176 can change conformation, controlling exchange of these ligands. The side chain of the mutated Phe135 in DhaA14 and DhaA15 was modelled in one conformation and most probably does not have the opportunity to change its position. It was found

that the bulky side chain of Phe135 almost completely blocks the small side tunnel in the mutated enzymes, suggesting that the main tunnel may still be the major pathway for the exchange of ligands in DhaA mutants.

The authors thank Mikalai Lapkouski for his help during the diffraction measurements. This work was supported by the Ministry of Education of the Czech Republic (MSM6007665808, LC06010), the Czech Science Foundation (310/09/1407), the Academy of Sciences of the Czech Republic (AV0Z60870520), the OptiCryst project of the 7th EU Framework and the 'Factoría Española de Cristalización', Consolider-Ingenio 2010 project (MEC). We are grateful to the X11 Consortium for Protein Crystallography for access to their facility.

References

Allen, F. H. (2002). *Acta Cryst.* B**58**, 380–388.
Banas, P., Otyepka, M., Jerabek, P., Petrek, M. & Damborsky, J. (2006). *J. Comput. Aided Mol. Des.* **20**, 375–383.
Bosma, T., Damborsky, J., Stucki, G. & Janssen, D. B. (2002). *Appl. Env. Microbiol.* **68**, 3582–3587.
Bosma, T., Kruizinga, E., Bruin, E. J. D., Poelarends, G. J. & Janssen, D. B. (1999). *Appl. Environ. Microbiol.* **65**, 4575–4581.
Brünger, A. T. (1993). *Acta Cryst.* D**49**, 24–36.
Campbell, D. W., Muller, C. & Reardon, K. F. (2006). *Biotechnol. Lett.* **28**, 883–887.
Chen, V. B., Arendall, W. B., Headd, J. J., Keedy, D. A., Immormino, R. M., Kapral, G. J., Murray, L. W., Richardson, J. S. & Richardson, D. C. (2010). *Acta Cryst.* D**66**, 12–21.
Chovancova, E., Kosinski, J., Bujnicki, J. M. & Damborsky, J. (2007). *Proteins*, **67**, 305–316.
Collaborative Computational Project, Number 4 (1994). *Acta Cryst.* D**50**, 760–763.
DeLano, W. L. (2002). *The PyMOL Molecular Viewer.* http://www.pymol.org.
Ducruix, A. & Giegé, R. (1999). *Crystallization of Nucleic Acids and Proteins: A Practical Approach*, 2nd ed. Oxford University Press.
Emsley, P., Lohkamp, B., Scott, W. G. & Cowtan, K. (2010). *Acta Cryst.* D**66**, 486–501.
Gray, K. A., Richardson, T. H., Kretz, K., Short, J. M., Bartnek, F., Knowles, R., Kan, L., Swanson, P. E. & Robertson, D. E. (2001). *Adv. Synth. Catal.* **343**, 607–616.
Janssen, D. B. (2004). *Curr. Opin. Chem. Biol.* **8**, 150–159.
Janssen, D. B., Dinkla, I. J. T., Poelarends, G. J. & Terpstra, P. (2005). *Environ. Microbiol.* **7**, 1868–1882.
Janssen, D. B., Pries, F. & Ploeg, J. R. (1994). *Annu. Rev. Microbiol.* **48**, 163–193.
Janssen, D. B. & Schanstra, J. P. (1994). *Curr. Opin. Biotechnol.* **5**, 253–259.
Klvana, M., Pavlova, M., Koudelakova, T., Chaloupkova, R., Dvorak, P., Prokop, Z., Stsiapanava, A., Kuty, M., Kuta-Smatanova, I., Dohnalek, J., Kulhanek, P., Wade, R. C. & Damborsky, J. (2009). *J. Mol. Biol.* **392**, 1339–1356.
Krissinel, E. & Henrick, K. (2004). *Acta Cryst.* D**60**, 2256–2268.
Kulakova, A. N., Larkin, M. J. & Kulakov, L. A. (1997). *Microbiology*, **143**, 109–115.
Murshudov, G. N., Vagin, A. A. & Dodson, E. J. (1997). *Acta Cryst.* D**53**, 240–255.
Nardini, M. & Dijsktra, B. W. (1999). *Curr. Opin. Struct. Biol.* **9**, 732–737.
Newman, J., Peat, T. S., Richard, R., Kan, L., Swanson, P. E., Affholter, J. A., Holmes, I. H., Schindler, J. F., Unkefer, C. J. & Terwilliger, T. C. (1999). *Biochemistry*, **38**, 16105–16114.
Oakley, A. J., Klvana, M., Otyepka, M., Nagata, Y., Wilce, M. C. J. & Damborsky, J. (2003). *Biochemistry*, **43**, 870–878.
Ollis, D. L., Cheah, E., Cygler, M., Dijkstra, B., Frolow, F., Franken, S. M., Harel, M., Remington, S. J., Silman, I., Schrag, J., Sussman, J. L., Verschueren, K. H. G. & Goldman, A. (1992). *Protein Eng.* **5**, 197–211.
Otwinowski, Z. & Minor, W. (1997). *Methods Enzymol.* **276**, 307–326.
Otyepka, M. & Damborsky, J. (2002). *Protein Sci.* **11**, 1206–1217.
Pavlova, M., Klvana, M., Prokop, Z., Chaloupkova, R., Banas, P., Otyepka, M., Wade, R. C., Tsuda, M., Nagata, Y. & Damborsky, J. (2009). *Nature Chem. Biol.* **5**, 727–733.
Petrek, M., Otyepka, M., Banas, P., Kosinova, P., Koca, J. & Damborsky, J. (2006). *BMC Bioinformatics*, **7**, 316.
Prokop, Z., Damborsky, J., Nagata, Y. & Janssen, D. B. (2004). Patent WO/2006/079295 A2.
Prokop, Z., Damborský, J., Opluštil, F., Jesenská, A. & Nagata, Y. (2005). Patent WO/2006/128390 A1.
Prokop, Z., Oplustil, F., DeFrank, J. & Damborsky, J. (2006). *Biotechnol. J.* **1**, 1370–1380.
Schindler, J. F., Naranjo, P. A., Honaberger, D. A., Chang, C.-H., Brainard, J. R., Vanderberg, L. A. & Unkefer, C. J. (1999). *Biochemistry*, **38**, 5772–5778.
Sheldrick, G. M. (2008). *Acta Cryst.* A**64**, 112–122.
Stsiapanava, A., Koudelakova, T., Lapkouski, M., Pavlova, M., Damborsky, J. & Kuta Smatanova, I. (2008). *Acta Cryst.* F**64**, 137–140.
Stucki, G. & Thuer, M. (1995). *Environ. Sci. Technol.* **29**, 2339–2345.
Swanson, P. E. (1999). *Curr. Opin. Biotechnol.* **10**, 365–369.
Teng, T.-Y. (1990). *J. Appl. Cryst.* **23**, 387–391.
Vagin, A. & Teplyakov, A. (1997). *J. Appl. Cryst.* **30**, 1022–1025.
Vaguine, A. A., Richelle, J. & Wodak, S. J. (1999). *Acta Cryst.* D**55**, 191–205.